Dynamic modification of the fragmentation of autoionizing states of O_2^+

W. Cao,[1] G. Laurent,[1] S. De,[1] M. Schöffler,[2] T. Jahnke,[3] A. S. Alnaser,[4] I. A. Bocharova,[2] C. Stuck,[3] D. Ray,[1] M. F. Kling,[1] I. Ben-Itzhak,[1] Th. Weber,[2] A. L. Landers,[5] A. Belkacem,[2] R. Dörner,[3] A. E. Orel,[6] T. N. Rescigno,[2] and C. L. Cocke[1]

[1]*J. R. Macdonald Laboratory, Department of Physics, Kansas State University, Manhattan, Kansas 66506, USA*

[2]*Lawrence Berkeley National Laboratory, Chemical Sciences, Berkeley, California 94720, USA*

[3]*Institut für Kernphysik, University of Frankfurt, D-60438 Frankfurt, Germany*

[4]*Physics Department, American University of Sharjah, Sharjah, United Arab Emirates*

[5]*Department of Physics, Auburn University, Auburn, Alabama 36849, USA*

[6]*Department of Applied Science, University of California, Davis, California 95616, USA*

(Received 13 September 2011; published 10 November 2011)

The dynamic process of fragmentation of excited states of the molecular oxygen cation is investigated in a two-part study. First, using monochromatic 41.6 eV radiation and cold-target recoil-ion momentum spectroscopy detection of $O^+ + O^+$ ion pairs and associated electrons, we establish that this channel is populated only by an indirect process enabled by autoionization of excited oxygen atoms and identify the final active potential curves. Second, we probe the dynamics of this process using an attosecond pulse train of 35–42 eV EUV followed by an intense IR laser pulse. The results are compared with a model calculation.

DOI: 10.1103/PhysRevA.84.053406 PACS number(s): 34.50.Rk, 33.80.Rv, 42.65.Ky

I. INTRODUCTION

The tracking of the dynamics of wave-packet motion in small molecules using pump-probe timing, with infrared pump and infrared probe, is now a mature subject [1,2]. The use of EUV as the pump, a more recent development [3–7], has the advantage over the IR pump that the EUV can populate, via a single-photon process, a range of excited states of various ionization states of the molecule. When high-order-harmonic generation (HHG) is used to generate the EUV, the resulting radiation is in the form of a short attosecond pulse train (APT) [8–10], which can be made short enough (below 10 fs) to track vibrational motion even in light molecules. Such an APT still retains some spectral resolution, allowing the experimentalist some degree of control over the range of excitation generated by the pump.

In this work we fragment the oxygen molecule with an APT. It is well known that the fragmentation of any oxygen-bearing diatomic molecule can produce autoionizing excited states of neutral atomic oxygen fragments [11–14]. Since the autoionization usually occurs on a time scale longer than that for fragmentation, the population of cation states of the molecule which dissociate to a charged ion plus autoionizing atomic oxygen atoms ultimately results in the observation of ion pairs in the dication channel. One of the pioneering EUV-IR pump-probe experiments on molecular oxygen [4] explored the dynamics of this process, and argued that the autoionization of the molecule was not only interrupted by a delayed IR pulse, but that this pulse actively participated in the process by adding a photon of energy to the autoionization electron. Photoelectron spectra were interpreted to indicate that only when the spontaneous process became energetically allowed could this mechanism proceed. In this work we probe this system further by observing the kinetic-energy release (KER) in the $O^+ + O^+$ channel as a function of the delay between the EUV populating pulse and the IR probe pulse, and proposing a specific path to interpret the result. We observe a large increase in the KER when the IR probe arrives, which we interpret to mean that the evolution from a specific cation potential-energy curve (PEC) to a dication PEC is hastened by the arrival of the IR.

There have been numerous previous studies of the production of electron or ion pairs from the ionization of molecular oxygen. The high-resolution spectra and associated analysis by Lundquist *et al.* [15] of the KER of $O^+ + O^+$ pairs identified the major channels through which the dication breaks if the excitation level exceeds ~40 eV (measured from the ground state of the neutral; see Fig. 1). This work has been the starting point for the interpretation of a number of experiments on KER spectra of the dication generated from a variety of excitation processes [4,16]. The important role of autoionizing channels populated by photoionization was first studied by Price *et al.* [12], as well as Hsieh *et al.* [13].

II. MONOENERGETIC BEAM SPECTRA

In order to be able to interpret KER spectra obtained with the broadband EUV from harmonic generation, we have first taken cold-target recoil-ion momentum spectroscopy (COLTRIMS) spectra with a monochromatic photon beam from the Advanced Light Source (ALS) at Lawrence Berkeley National Laboratory. The technique is described in detail elsewhere [17,18]. A monochromatic 41.6 eV EUV beam is directed onto a supersonic jet of molecular oxygen. The momenta of all ions and electrons emerging from the interaction region are recorded in coincidence for each event. At a photon energy of 41.6 eV one can make a direct double ionization to a dication state only for the $A^3\Sigma_u$ and $X^1\Sigma_g$ states (see Fig. 1). At the Franck-Condon (FC) distance of 2.27 a.u., population of the $X^1\Sigma_g$ is mainly to bound states, and population of the $A^3\Sigma_u$ state is barely possible. The major dissociating states of the dication start with the $W^3\Delta_u$ [13] and at 41.6 eV one cannot reach them. Thus there is essentially no direct dissociative double ionization of molecular oxygen at this photon energy. This is in contrast to the situation for CO, which we reported earlier [7].

Nevertheless, a strong yield of $O^+ + O^+$ ion pairs and electron pairs is observed. Figure 2 shows a density plot of the yield measured in the $O^+ + O^+ + e^- + e^-$ channel (four-particle coincidence). In Fig. 2(b), the energy of one

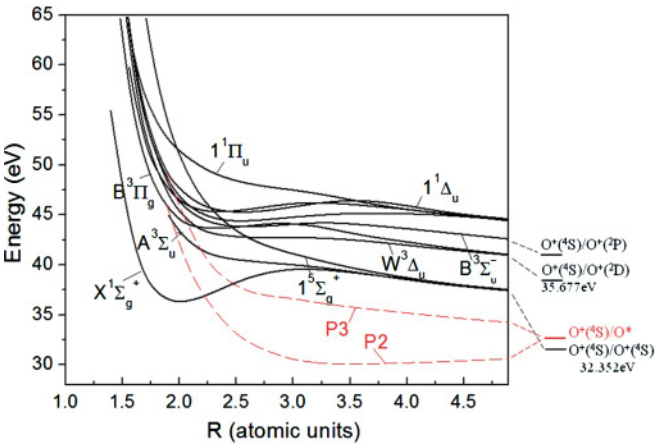

FIG. 1. (Color online) Partial energy-level diagram for the dication of O_2 (adapted from Ref. [15]). The red-dashed lines labeled as $P2$ and $P3$ indicate the calculated doubly excited cation states which can autoionize into the $O^+(^4S)/O^+(^4S)$ limit (see text).

electron (E_1) is plotted versus the energy of the other one (E_2). Since there is nearly no direct population of this channel, we identify all events as resulting from the production of a cation of O_2 which dissociates to $O^+ + O^*$, with the O^* then autoionizing after fragmentation to O^+ and an electron. Labeling, for the moment, the autoionization electron E_2 and the photoelectron E_1, the strong vertical stripes appearing near $E_2 = 0.4$, 0.7, and 1.6 eV are due to autoionization lines emitted from excited O neutrals after dissociation of the molecule has taken place. The value of E_1 along each line gives the spectrum of the associated photoelectron, and thus serves to identify the location of the initially populated PEC on which the dissociation of the cation occurs prior to autoionization. Of course, since we have no way to distinguish the autoionization electron from the photoelectron, the same features appear with E_1 and E_2 interchanged (symmetry about the diagonal). The spectrum of Fig. 2(b) is closely related to Fig. 2 of Ref. [11], and detailed identifications of the autoionization lines are given in that work.

In Fig. 2(a), the KER of the ion pair is plotted versus the sum energy of the two electrons. In such a plot, all events

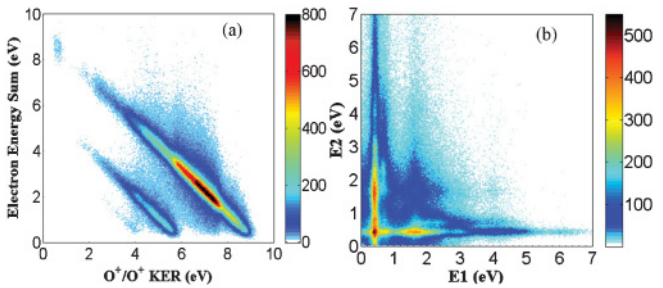

FIG. 2. (Color online) Correlation plots of the four-particle ($O^+ + O^+$ and the associated two electrons) coincidence experiment. (a) Density plot of the energy sum of the two electrons versus the $O^+ + O^+$ KER. (b) Density plot of the kinetic energy of the designated second electron (E_2) versus that of the first electron (E_1). The data were taken at the COLTRIMS station at the ALS with a photon energy of 41.6 eV.

leading to a particular final state of $O^+ + O^+$ are energetically constrained to a diagonal line. The energy difference between the photon energy and the four particles' sum energy will determine the final dissociation limit of the corresponding process. There are two diagonal lines in Fig. 2(a) which show that two autoionizing channels are involved. The higher energy line, the main one, corresponds to the $^4S/^4S$ final limit of $O^+ + O^+$ (32.352 eV). It is populated through an autoionizing state(s) of the cation $O^*(\ldots 2p^3[^2D]3p)/O^+(^4S)$ (and similar states; see Ref. [11]), which then decays to the $^4S/^4S$ limit. From the electron spectra of Fig. 2(a) we deduce that the energy of the autoionizing state(s) near the FC radius of 2.27 a.u. is near 39 eV, which produces the observed photoelectron energy E_1 near 1.8 eV. This corresponds to the $A1$ and $A2$ lines identified by Feifel *et al.* [11]. The lower energy line with a much weaker population corresponds to a final dissociation limit of ~35.6 eV, which can be identified as a final dication state correlated to the $O^+(^4S)/O^+(^2D)$ limit (see Fig. 1). This is similar to the $A3$ and $A4$ lines identified by Feifel *et al.* [11]. In fact, there is a wide range of E_1 along this line, suggesting that several PEC of the cation participate. The lack of any sharp features in E_1 also suggests that the participating PEC(s) are fairly steep in the FC region.

III. THEORETICAL CALCULATIONS

To support the interpretation of the measured data and better characterize the principal autoionizing excited state(s) of the cation involved, we carried out configuration-interaction (CI) calculations on the electronic states of O_2^+, with a view toward identifying inner-valence excited states that can be produced from ground-state ($^3\Sigma_g^-$) O_2 by absorption of a single EUV photon. A molecular orbital basis for the calculations was constructed by carrying out multiconfiguration self-consistent field calculations on the ground state of the dication with an augmented, correlation-consistent-polarized, valence triple-ζ basis on the oxygens. For the CI calculations, we kept the core oxygen 1s orbitals doubly occupied and included all single excitations from a multireference, complete active space (CAS) set of configurations using eight molecular orbitals (oxygen 2s and 2p) in the active space.

The independent-particle (Koopmans') model generally breaks down for inner-valence singly charged ions, which are characterized by strong configuration mixing and numerous curve crossings. In the FC region, removal of an inner-valence electron—in this case from an O 2s ($2\sigma_g$ or $2\sigma_u$) orbital—produces a number of excited states with varying amounts of valence character. States in the energy range of interest (~39 eV in the FC region) here involve a $2\sigma_g$ vacancy. The calculations show two such states of symmetry, $^4\Sigma_g^-$ and $^2\Delta_g$, respectively, which lie just above the ground state of the dication in the FC region. The PECs for both states are shown in Fig. 1. The dominant valence configuration for both states is $(\ldots 2\sigma_g^{-1}\pi_g^2)$. As the internuclear separation is increased beyond 2.27 a.u., there are numerous crossings among the excited states and the two inner-valence states rapidly lose their valence character as they take on more Rydberg character. To arrive at the plotted curves, we examined the dominant CI coefficients as a function of R, allowing states to cross if there was little interaction, but following the adiabatic curve

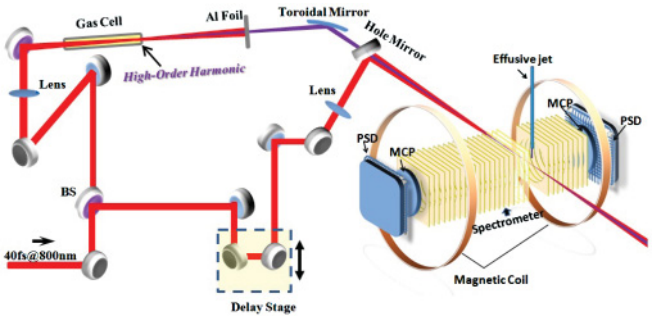

FIG. 3. (Color online) Schematic of the pump-probe experimental apparatus.

otherwise [14]. The $^4\Sigma_g{}^-$ and $^2\Delta_g$ states cross the O_2^{2+} ground state near $R = 66$ a.u. and can then autoionize. It is likely that the $^4\Sigma_g{}^-$ and $^2\Delta_g$ inner-valence states correspond to the "$P2$" and "$P3$" states observed by Feifel *et al.* [11], with the higher-energy $P3$ state most likely providing the dominant indirect ionization route observed in the COLTRIMS spectra. We note that, according to the observations of Feifel *et al.*, the $P3$ state feeds both the $A1$ ($\ldots 2p^3[^2D]3p$, ^3D) and "$A2$" O^* autoionizing states near 0.4 and 0.5 eV, respectively. The data of Fig. 2(b) suggests that the $A1$ channel is dominant. The pump-probe data described below confirms this assignment.

IV. PUMP-PROBE EXPERIMENT

Armed with an understanding of the origin of $O^+ + O^+$ pairs from irradiation of molecular oxygen in the 40-eV-and-below region of excitation, we now proceed to explore the dynamics of the fragmentation process. HHG was used to produce an APT of EUV light. Since the APT has a pulse train structure extending over a shorter time (we estimate 10–20 fs here) than the pulse duration of the driving laser field, a time-resolved experiment can be conducted to explore the dynamic process of fragmentation on the time scale of the probe pulse. Figure 3 shows the schematic of our pump-probe experimental setup. An 800 nm Ti:sapphire laser pulse with a repetition rate of 1 kHz and a pulse duration of 40 fs was delivered to the EUV-IR interferometer. Part of the IR beam was focused into a semi-infinite gas cell containing 30 torr of argon gas to generate high harmonics serving as the EUV pump. A 200 nm aluminum foil was placed after the gas cell to eliminate the residual IR beam. The EUV beam was then focused to the target jet of a COLTRIMS system [17,18] by a toroidal reflector. The usual COLTRIMS supersonic jet was replaced by a diffusive jet to raise the target density. Another portion of the IR pulse was reflected by the beam splitter (BS) before the harmonic generation and recombined with the EUV, after an appropriate and adjustable delay, to provide the probe beam. The focused intensity of the probe was below 10^{12} W/cm^2. We deduced the harmonic content of the APT using the photoelectron spectrum it generated from an Ar target. The photon energy is the sum of the observed photoelectron energy and the 15.76 eV first ionization potential of Ar. Figure 4 shows the measured photoelectron spectrum from Ar, which reveals radiation mainly from the 21st (32.5 eV) through 27th (41.9 eV) harmonics, with dominance by the 25th (38.8 eV).

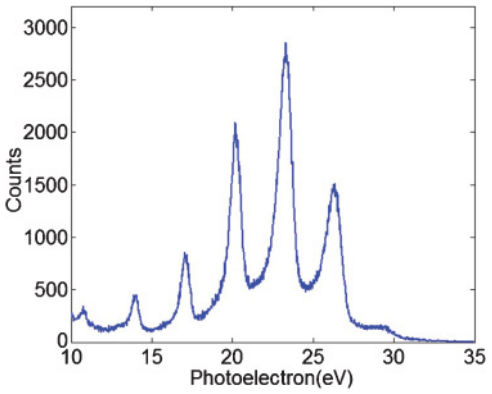

FIG. 4. (Color online) Photoelectron spectrum from EUV interaction with an argon target.

In Fig. 5 we show the KER in the $O^+ + O^+$ channel as a function of the pump-probe delay. At negative delay, when IR comes before XUV, a single broad peak near a KER of 6.8 eV is seen. This spectrum is the same as was obtained with no IR. Such a KER would result from states of the cation lying, in the FC region, near an excitation of 39 eV. Similar to the data of Fig. 2(a), this channel could be identified as due to the following process: $O_2 + h\nu \rightarrow O^+/O^* + e^- \rightarrow O^+(^4S)/O^+(^4S) + e^- + e^-$.

The fragmentation takes place first in an autoionizing excited state of the cation, hereafter referred to as AIC. The energetic properties of this state are known in the FC region, where it must be near 39 eV from Fig. 2(a), and at large internuclear distances where it must lie at 32.75 eV. The calculated AIC $P3$ described in the previous section and shown in Fig. 1 as a dashed red line has these properties. The AIC $P2$, also calculated and shown in Fig. 1, has too low an energy in the FC region to match the experimental data.

When the IR pulse arrives, the experimental KER is seen to increase abruptly to >10 eV. This increase then decays slowly with a lifetime near 250 fs. We interpret this to result from the removal of the most loosely bound electron from the AIC state, resulting in the population of a dissociative dication state.

For positive delays, the total KER will be the summation of the kinetic energy accumulated on AIC before the IR

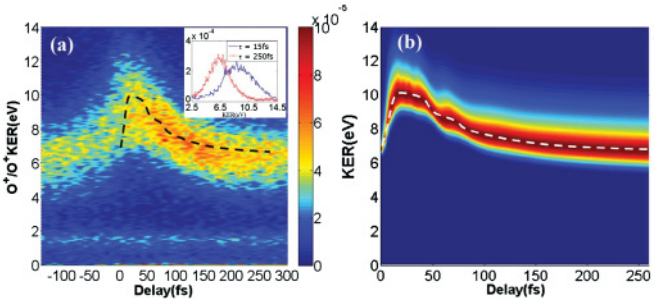

FIG. 5. (Color online) (a) Experimental density plot of KER versus delay of IR pulse with respect to the EUV pulse. Inset shows the projections of the spectra at different delays. (b) Calculated density plot of KER versus delay for the AIC $P3$. The dashed line shows the centroid of the calculated plot and is used to compare with the experimental data in panel (a).

pulse arrives and the kinetic energy accumulated on the dication curve after the IR pulse arrives. For large internuclear distances, both the AIC and dication curves are well known. The lack of Coulomb repulsion in the AIC state leads to a nearly flat potential curve, while the dication curve retains a repulsive Coulomb tail. Thus we expect to see an increase in the $O^+ + O^+$ KER coming from the extra Coulomb energy of the ion pair. The larger the delay, the larger the internuclear distance the AIC wave packet can reach prior to ionization and the smaller the KER increase.

We model the KER versus delay curve quantitatively. As indicated above, outside the FC region, the AIC states are well described as dication core states with a loosely bound $3s$ or $3p$ electron added. The dication core state of the AIC should be one which fragments to the $O^+ + O^+ {}^4S/{}^2D$ state, so as to provide the core energy necessary for ultimate autoionization for the uninterrupted fragmentation. We assume an initial population by the APT of a wave packet on the $P3$ AIC potential curve shown in Fig. 1. The shape of this packet is that of the lowest vibrational state of the neutral oxygen molecule. Using a numerical solution to the one-dimensional time-dependent Schrödinger equation, we allow this wave packet to propagate on the $P3$ AIC until the IR probe pulse arrives. At this point, the wave packet is assumed to be promoted to the dication core state, from which it completes its fragmentation. The KER is calculated from the asymptotic form of the final wave packet. Although many dication states could participate, in reality we choose the $W^3\Delta_u$ PEC from the ${}^4S/{}^2D$ manifold, the lowest-lying state with the correct asymptote, as the final dication state. The resulting plot of KER versus delay is shown in Fig. 5(b). While there is some fine structure in the plot for delays less than 50 fs, the 40 fs pulse duration of the probe pulse does not allow us to resolve this structure experimentally. The centroid of the calculated KER is shown as a light dashed line in Fig. 5(b). The same line is shown as a heavy dashed line superimposed on the data of Fig. 5(a). In this simulation, the abrupt increase on the KER for short delays is caused by the fact that the AIC $P3$ is much steeper than the $W^3\Delta_u$ PEC for small internuclear distance ($R < 3.0$). It is then followed by a slow KER decreasing over 250 fs corresponding to a large internuclear behavior as discussed before. The qualitative agreement shown between calculation and experiment suggests the validity of the assumption of the participating curves and supports the interpretation of the dynamics of this process. We have also modeled the KER versus delay using the $P2$ curve in Fig. 1 and found that it gives a rather poor match to the experimental data, with peak KER values at short delays much larger than that observed and smaller KER values at long delay times.

Although the main feature of the O_2 dynamic study results from the dissociation through the ${}^4S/{}^2D$ asymptote as discussed above, other dissociation limits can also be involved due to the coupling between different electronic curves at the crossing point in the presence of the laser field. The inset in Fig. 5(a) shows the KER spectra at two different delays (15 and 250 fs). When the IR pulse comes slightly after the XUV pulse, the KER spectrum goes up to 11 eV with a bandwidth of 5.2 eV, while for a large delay (250 fs), the bandwidth of the KER is only 3.6 eV. This can be qualitatively explained by considering the coupling between different dication states. The initially populated wave packet on the AIC state is moving outward. At $R \sim 2.6$ a.u. (corresponding to a delay $\sim$13 fs), the $1\,{}^5\Sigma_g{}^+$ and $W^3\Delta_g$ dication curves cross. If the IR pulse arrives at this delay, it can do two things. First, the IR pulse can promote the system onto the $W^3\Delta_g$ dication state; second, the IR pulse can open up the crossing point of $1\,{}^5\Sigma_g{}^+$ and $W\,{}^3\Delta_g$ states so that the $O_2{}^{2+}$ can dissociate via the $1\,{}^5\Sigma_g{}^+$ curve and reach the ${}^4S/{}^4S$ limit instead of the ${}^4S/{}^2D$ limit. Therefore, higher KER and broader spectrum will be expected. For large delays, where the internuclear distance is well beyond the crossing point of the $1\,{}^5\Sigma_g{}^+$ and $W^3\Delta_g$ states, no coupling is involved and the $O_2{}^{2+}$ can only dissociate into the ${}^4S/{}^2D$ limit, which gives a relatively narrower KER bandwidth.

V. SUMMARY AND CONCLUSION

In conclusion, we have studied the dynamic process of the fragmentation of an autoionization cation state(s) in oxygen molecules. The study involves two parts. First, a 41.6 eV monochromatic photon beam from the ALS was used to ascertain that, for photon energies below 41 eV, the yield of $O^+ + O^+$ ion pairs from single-photon absorption is dominated by an indirect process, namely, fragmentation of a molecular state of the cation followed by autoionization of the neutral fragment. The dominant such state is found to have energy near 39 eV in the FC region, and near 32.8 eV at large internuclear distances. Theoretical calculations identify this state as a ${}^2\Delta_g$ molecular cation ($P3$ in Fig. 1) having a predominantly $2\sigma_g{}^{-1}$ character in the FC region and correlating with $O^+({}^4S)/O^*(3p'[{}^3D])$ at large internuclear separation. Second, the dynamics of the fragmentation of this state was investigated in a pump-probe experiment. The fragmentation process was interrupted by a short IR pulse, which served to remove the most loosely bound electron from the cation state, producing a dissociating dication state which asymptotically reaches the $O^+({}^4S)/O^+({}^2D)$ limit. The experimental observation was that the kinetic-energy release of the ion pair was increased substantially by the arrival of the IR pulse, by an amount which decayed slowly as a function of delay between APT and IR pulses. Using the autoionizing cation state obtained from CI calculations and reasonable assumptions concerning the form of the dication state involved, a model for the fragmentation process was evaluated which showed good agreement with the experiment. The behavior of this process is very similar to one reported earlier by us for CO, except that in this case *only* the indirect autoinizing route to production of fragments from the dication is possible. It is becoming increasingly clear in EUV(pump)-IR(probe) experiments, that the general situation found here is a recurrent theme. The main effect of the IR probe is to remove loosely bound electrons from excited states of cation (or higher charged) molecules created by the EUV, thereby boosting the system to the next higher charge state and enhancing the KER of the fragments.

ACKNOWLEDGMENTS

This work was supported by Chemical Sciences, Geosciences and Biosciences Division, Office of Basic Energy Sciences, Office of Science, U.S. Department of Energy. W.C.

was supported by the National Science Foundation under Grant No. CHE-0822646. G.L. was supported by the US Army Research Office under Grant No. W911NF-07-1-0475. M.F.K. was partially supported by the German Science Foundation via the Emmy-Noether program and the Cluster of Excellence: Munich Center for Advanced Photonics. M.S. gratefully acknowledges support by the Alexander von Humboldt foundation.

[1] Th. Ergler, A. Rudenko, B. Feuerstein, K. Zrost, C. D. Schröter, R. Moshammer, and J. Ullrich, Phys. Rev. Lett. **95**, 093001(2005).
[2] A. S. Alnaser *et al*., Phys. Rev. A **72**, 030702(R) (2005).
[3] E. Gagnon, P. Ranitovic, X. M. Tong, C. L. Cocke, M. M. Murnane, H. C. Kapteyn, and A. S. Sandhu, Science **317**, 1374 (2007).
[4] A. S. Sandhu, E. Gagnon, R. Santra, V. Sharma, W. Li, Ph. Ho, P. Ranitovic, C. L. Cocke, M. M. Murnane, and H. C. Kapteyn, Science **322**, 1081 (2008).
[5] I. Thomann, R. Lock, V. Sharma, E. Gagnon, S. T. Pratt, H. C. Kapteyn, M. M. Murnane, and W. Li, J. Phys. Chem. **112**, 9382 (2008).
[6] J. M. Glownia *et al*., Opt. Express **18**, 17620 (2010).
[7] W. Cao *et al*., Phys. Rev. A **82**, 043410 (2010).
[8] P. M. Paul, E. S. Toma, P. Breger, G. Mullot, F. Augé, Ph. Balcou, H. G. Muller, and P. Agostini, Science **292**, 1689 (2001).
[9] P. Antoine, A. L'Huillier, and M. Lewenstein, Phys. Rev. Lett. **77**, 1234 (1996).
[10] Y. Mairesse *et al*., Science **28**, 1540 (2003).
[11] R. Feifel, J. H. D. Eland, and Edvardsson, J. Chem. Phys. **122**, 144308 (2005).
[12] S. D. Price and J. H. D. Eland, J. Phys. B **24**, 4379 (1991).
[13] S. Hsieh and J. H. D. Eland, J. Phys. B **29**, 5795 (1996).
[14] T. Osipov *et al*., Phys. Rev. A **81**, 011402 (2010).
[15] M. Lundqvist, D. Edvardsson, P. Baltzer, M. Larsson, and B. Wannberg, J. Phys. B **29**, 499 (1996).
[16] A. S. Alnaser, S. Voss, X. M. Tong, C. M. Maharjan, P. Ranitovic, B. Ulrich, T. Osipov, B. Shan, Z. Chang, and C. L. Cocke, Phys. Rev. Lett. **93**,113003 (2004).
[17] J. Ullrich, R. Moshammer, R. Dörner, O. Jagutzki, V. Mergel, H. Schmidt-Böcking, and L. Spielberger, J. Phys. B **30**, 2917 (1997).
[18] R. Dörner, V. Mergel, O. Jagutzki, L. Spielberger, J. Ullrich, R. Moshammer, and H. Schmidt-Böcking, Phys. Rep. **330**, 95 (2000).